Sensors and Actuators A 299 (2019) 111628

Contents lists available at ScienceDirect

Sensors and Actuators A: Physical

journal homepage: www.elsevier.com/locate/sna

$GdVO_4$:Er^{3+}/Yb^{3+} nanocrystalline powder as fluorescence temperature sensor. Application to monitor the temperature of an electrical component

Franzette Paz-Buclatin[a,*], Fernando Rivera-López[b], Oswaldo González[b], Inocencio R. Martín[a,c], Leopoldo L. Martin[a], Dragana J. Jovanović[d]

[a] Departamento de Física, Universidad de La Laguna, Apdo. 456. E-38200 San Cristóbal de La Laguna, Santa Cruz de Tenerife, Spain
[b] Departamento de Ingeniería Industrial, Escuela Superior de Ingeniería y Tecnología, Universidad de La Laguna, Apdo. 456, E-38200 San Cristóbal de La Laguna, Santa Cruz de Tenerife, Spain
[c] Instituto Universitario de Materiales y Nanotecnología (IMN), Universidad de La Laguna, Apdo. 456, E-38200 San Cristóbal de La Laguna, Santa Cruz de Tenerife, Spain
[d] Vinča Institute of Nuclear Sciences, University of Belgrade, P.O. Box 522, 11001 Belgrade, Serbia

ARTICLE INFO

Article history:
Received 16 July 2019
Received in revised form 4 September 2019
Accepted 17 September 2019
Available online 21 September 2019

Keywords:
Nanoparticle
$GdVO_4$
Erbium
Temperature
Optical sensor

ABSTRACT

The temperature sensing properties of an Er^{3+}/Yb^{3+} co-doped $GdVO_4$ nanocrystalline powder were studied. The down-conversion emission spectrum of the sample was observed under excitation at 457 nm. Two methods were used to calibrate the temperature of the sample: one based on the Fluorescence Intensity Ratio (FIR) technique and the other using the fluorescence lifetime of the thermally-coupled energy levels of Er^{3+}. The relative sensitivities for each method were calculated and it was found out that the FIR-based temperature sensor has higher sensitivity (1.17% K^{-1}) than the lifetime-based sensor (0.24% K^{-1}). Furthermore, a temperature uncertainty of 0.37 K was obtained for the FIR-based sensor. The $GdVO_4$ nanoparticles were also used to study the change in temperature of an electrical component when it is operating and not.

1. Introduction

Nowadays, a huge variety of devices are available for temperature measurements in diverse fields, such as science and engineering. However, conventional instruments are inefficient in some hostile environments as, for example, corrosive ambient. For this reason, it is necessary to investigate new sensors that can be adapted in all types of environments. Optical temperature sensors are considered as an excellent solution, in which luminescence is used to translate optical signals into temperature measurements [1]. These devices are oriented to replace classical sensors in the fields of nano-engineering, bio-imaging, therapeutics [2], power stations, oil refineries, coal mines or building fire detections [3]. Among their advantages are the rapid response, non-invasive operation, high spatial resolution, high accuracy, high temperature sensitivity, freedom from electro-magnetic interference and noise immunity because no electrical currents flow at the sensing point.

In order to develop an effective optical temperature sensor, it is necessary to select a suitable optically active ion and host matrix. The results obtained from temperature sensing using active hosts doped with erbium ions suggest that erbium is a good candidate as a dopant ion [4]. It is well known that trivalent erbium ion (Er^{3+}) can emit two intense green emissions at around 525 and 550 nm, corresponding to $^2H_{11/2} \rightarrow {}^4I_{15/2}$ and $^4S_{3/2} \rightarrow {}^4I_{15/2}$ transitions, respectively. The energy level gap of $^2H_{11/2}$ and $^4S_{3/2}$ is very small, located in the range of 200 cm^{-1} - 2000 cm^{-1} which fulfill the requirement for it to be used as an optical temperature sensor. The small separation between these levels implicates a high probability of non-radiative transitions between them.

There are various sensing methods that take advantage of this feature of rare-earth ions. In particular, two methods will be studied in this work: the FIR technique and the fluorescence lifetime-based temperature calibration. These methods rely on the fact that the relative population of the two thermally-coupled energy levels can be affected by the variations of the environmental temperature according to the Boltzmann distribution law [5,6]. This in turn varies the relative fluorescence intensity of the emissions from these levels as well as their effective lifetime.

* Corresponding author.
E-mail address: fpazbucl@ull.es (F. Paz-Buclatin).

https://doi.org/10.1016/j.sna.2019.111628
0924-4247/

It is worth noting that the energy difference between the emitting levels is an important factor. This energy gap must be large enough in order to avoid overlapping, but if the separation is too large, the upper level cannot possess enough population in a certain temperature range and, in that case, the Boltzmann's distribution model is not useful to describe the electronic populations of the emitting levels [7]. In addition to these considerations, it is important to dope materials with relatively low concentration of Er^{3+} in order to avoid radiative energy transfer between Er^{3+} ions and to obtain large thermal sensitivities [8].

The FIR technique and fluorescence lifetime-based calibration can be considered as adequate noncontact temperature sensing methods, which can realize remote temperature measures at a distance from the object. FIR [9–12] and lifetime-based temperature calibration [13–15] has been extensively studied due to their various advantages. The main strength of these sensing methods are that they are based on the thermal equilibrium of the coupled levels so they present a good independence from external interferences, luminescence loss, and fluctuations of the source power [16–19]. Moreover, FIR has good measurement accuracy as well as resolution, broad temperature range [20] and requires low excitation power which reduces the self-heating [21].

The selection of an appropriate material is based on the high efficiency of the fluorescence signal and the good thermal stability of the material. In this sense, for example, fluoride glasses and crystals exhibit good fluorescence properties for being employed as temperature sensor, but the poor mechanical and chemical nature limits the practical application in high temperature measurement [22]. Moreover, they are very sensitive to oxygen surface contamination, which may influence their luminescence properties [23]. Although oxides can work well at high temperatures due to the stable chemical properties, a lower fluorescence efficiency could be observed because of the high energy phonon [24,25], which increases non-radiative de-excitation. In this work gadolinium orthovanadate ($GdVO_4$) nanopowder doped with Er^{3+}-Yb^{3+} is studied as possible candidate for temperature sensing. Nanoparticles are very interesting due to the reduced light scattering. $GdVO_4$ phosphor has interesting luminescent properties such as chemical stability and machine property. The matrix is very adequate because Gd^{3+} ion can be substituted with lanthanide ions because of the equal valence and similar ionic radius [26]. Besides, this material is considered as a promising host with relatively low phonon energy compared with oxides and close lattice matches to dopant ions [25,27].

In this work, the $GdVO_4$: Er^{3+}/Yb^{3+} downconversion emissions where studied in order to perform a temperature calibration through the FIR technique. Other works employing $GdVO_4$: Er^{3+}/Yb^{3+} sample study the upconversion emission instead to perform a temperature calibration via FIR [28,29]. However, observing downconversion requires lower pump power than the upconversion process, which in turn reduces the possibility of heating the sample from the laser itself instead from its surrounding medium. This is especially important when performing a temperature calibration of the sample.

After the calibration of the sample through the FIR technique, the optical sensor is evaluated by measuring the temperature of an electrical component.

2. Theoretical background

2.1. FIR technique

The FIR technique relies on the dependence of the sample temperature with the ratio of the fluorescence intensity of two thermally-coupled energy levels. The fluorescence intensity emitted from level 1 to level 0 at temperature T is given as [30]:

$$I_{1,0} = g_1\sigma_{1,0}\omega_{1,0}e^{-E_1/k_BT} \tag{1}$$

and from a higher level 2 to level 0 is:

$$I_{2,0} = g_2\sigma_{2,0}\omega_{2,0}e^{-E_2/k_BT} \tag{2}$$

where $I_{2,0}$ and $I_{1,0}$ are the integrated intensities corresponding to the fluorescence transitions from the upper level and from the lower level to the ground level respectively, g are the $(2J+1)$ degeneracies of the energy levels, σ are the emission cross-section, ω are the angular frequencies of the transition, E_1 and E_2 are the energy of the lower and upper level, respectively, k_B is Boltzmann's constant and T is the absolute temperature.

Taking into account Eqs. (1) and (2), the FIR of the two thermally coupled energy levels can be written as [31]:

$$R = \frac{I_{2,0}}{I_{1,0}} = \frac{g_2\sigma_{2,0}\omega_{2,0}}{g_1\sigma_{1,0}\omega_{1,0}}e^{-\Delta E/k_BT} = Be^{-\Delta E/k_BT} \tag{3}$$

where $B = g_2\sigma_{2,0}\omega_{2,0}/g_1\sigma_{1,0}\omega_{1,0}$ is the pre-exponential constant and ΔE is the energy gap between the thermally-coupled levels.

2.2. Temperature dependency of the fluorescence lifetime

The redistribution of population between the thermally-coupled levels due to a change in temperature not only affects the relative fluorescence intensity of the corresponding emissions but also the lifetime of these energy levels. When thermal equilibrium is achieved between these energy levels, their lifetimes will be the same and correspond to an effective lifetime τ, dependent on the temperature [32]. In particular, under the assumption that the rate of relaxation between the thermally-coupled energy levels due to rapid thermalization is very large compared with their spontaneous lifetimes, the effective lifetime is given as [33]:

$$\tau = \frac{g_1 + g_2e^{-\Delta E/k_BT}}{g_1A_1 + g_2A_2e^{-\Delta E/k_BT}} \tag{4}$$

where A_1 and A_2 are the sum of the probabilities of spontaneous emission from the lower and upper energy levels to all lower energy levels, respectively.

Depending on the ratio of the intrinsic lifetime of the two levels $\tau_1 = 1/A_1$ and $\tau_2 = 1/A_2$, the effective lifetime can increase or decrease with increasing temperature. Based on Eq. (4) it can be deduced that if $\tau_1 > \tau_2$, a decreasing effective lifetime is to be expected and vice-versa. Measurements of the effective lifetime can be obtained from either just one of the fluorescence wavelengths or over a bandwidth covering the decays from the thermalizing levels [34].

2.3. Relative sensor sensitivity

The relative sensitivity S_R is a very important parameter used to compare the performance of optical temperature sensors independent of their nature and is calculated as follows [35]:

$$S_R = \frac{1}{MP}\left|\frac{dMP}{dT}\right| \tag{5}$$

where MP is the parameter measured by the sensor. For the FIR technique, MP corresponds to the intensity ratio, and for the lifetime-based calibration it corresponds to the effective lifetime of the coupled energy levels.

Using Eq. (3), the relative sensitivity of a FIR-based sensor is given as:

$$S_{FIR} = \frac{1}{R}\left|\frac{dR}{dT}\right| = \frac{\Delta E}{kT^2} \tag{6}$$

From this equation, it is obvious that higher sensitivities are related to large energy differences between two thermalized levels. However, a too high energy gap can decrease the population and the intensity from the upper thermalized level. The interest of this parameter is the independency with the emission intensity, it only depends on the temperature and the energy gap.

On the other hand, using Eq. (4), the sensitivity of a fluorescence lifetime-based sensor is given as:

$$S_\tau = \frac{1}{\tau}\left|\frac{d\tau}{dT}\right| = \left(1 - \frac{1}{g_1 + g_2 e^{-\Delta E/k_B T}}\right) \left(\frac{A_1 - A_2}{g_1 A_1 + g_2 A_2 e^{-\Delta E/k_B T}}\right) \frac{\Delta E}{kT^2} \quad (7)$$

Another parameter of interest is the temperature uncertainty which refers to the minimum temperature change that can be detected by the sensor. It can be experimentally obtained by studying the statistical distribution of the measured temperatures.

3. Experimental

3.1. Synthesis of $GdVO_4$: Er^{3+}/Yb^{3+} sample

Nano-sized $Gd_{0.88}Er_{0.02}Yb_{0.1}VO_4$ particles were synthesized by cost-effective and easy to scale-up co-precipitation method by analogy to the method presented in Ref. [36]. Typically, first, an appropriate amount of NH_4VO_3 was dissolved into an aqueous solution of NaOH. The mixture of aqueous solutions of Gd^{3+}, Er^{3+} and Yb^{3+} ions in the corresponding stoichiometric ratio was added drop by drop in a solution with $VO_4{}^{3-}$ and immediately milk-white opalescent precipitate of $Gd_{0.88}Er_{0.02}Yb_{0.1}VO_4$ was formed. The obtained suspension was additionally stirred and heated at 60 ºC for one hour. Finally, the precipitate was separated from the suspension by centrifugation, washed out several times with distilled water and dried at 60 °C for 20 h. In order to improve crystallinity, the prepared powder was additionally annealed at 600 °C for two hours.

3.2. Sample characterization

The crystalline structure of the powder was studied over the 2θ range of 10°-90°, with a step size of 0.02° and a counting time of 0.7°min^{-1} by an X-ray diffractometer (XRD) Rigaku SmartLab (Cu-K$\alpha_{1,2}$ radiation, λ = 0.1540 nm) at room temperature.

3.3. Optical measurements

To perform the temperature calibrations, the powder sample was heated by placing it in the middle of a tubular furnace and the temperature was increased from room temperature (RT) to 370 K. A K-type thermocouple located near the sample and coupled to a temperature calibrator (Fluke 714) permits the reading of the exact temperature of the sample.

The FIR technique is based on the changes on the relative intensities between two bands of the emission spectrum. To obtain the emission spectra of the sample, the excitation was carried out with a 457 nm continuous laser, focalized onto the sample. The luminescence from the sample was filtered with a short-pass filter and then focalized at the tip of an optical fiber located at the opposite side of the furnace. The optical fiber was connected to a 0.3 m single grating spectrometer (Andor SR-3031-B) and the signal was measured with a cooled CCD detector (Newton DU920 N) with a resolution of 0.7 nm (~25 cm^{-1}) and an integration time of 1 s.

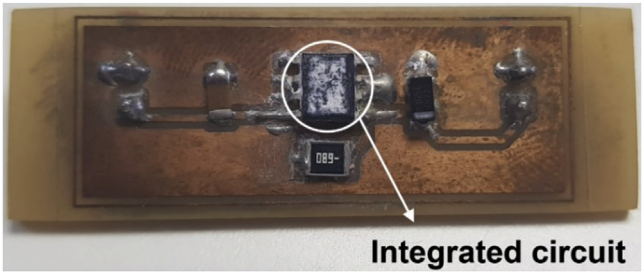

Fig. 1. Printed circuit board containing an integrated circuit to be analyzed. The GdVO4: Er^{3+}/Yb^{3+} nanoparticles are partially distributed on the surface of this electrical component (integrated circuit) for its use as a temperature sensor.

For the temperature calibration using the fluorescence lifetime, a 10 ns pulsed laser from an EKSPLA NT 342/3/UVE Optical Parametric Oscillator (OPO) was used to excite the sample at 457 nm. The emission was focalized towards the entrance slit of a TRIAX 180 monochromator coupled with a Hamamatsu R928 photomultiplier. The signal was then transmitted to a LeCroy Wavesurfer 424 digital oscilloscope which permits the visualization of the emission intensity as a function of time. The luminescence decay curves at 550 nm for different temperatures were recorded and analyzed in order to calibrate the temperature with the lifetime.

3.4. Application on an electrical component

Once the temperature calibration of the nanoparticles was performed and a sensing method was chosen, these nanoparticles were used to study how the temperature of an electrical component (integrated circuit) changes when it is operating. For this, the sample was distributed on the surface of the component as shown in Fig. 1 and the temperature was measured using the chosen calibration method.

Furthermore, an infrared image of the integrated circuit while operating was obtained using a FLIR InfraCAM infrared camera equipped with a focal plane array uncooled microbolometer with a resolution of 120 × 120 pixels.

4. Results

4.1. Structural characterization

XRD pattern of the $Gd_{0.88}Er_{0.02}Yb_{0.1}VO_4$ powder, together with standard data for single tetragonal zircon-type phase (ICDD card No. 01-086-0996) with the space group of I41/amd is shown in Fig. 2a. The absence of impurity phases compared to the reflection positions of standard data indicate that Er^{3+} and Yb^{3+} ions were successfully incorporated into the $GdVO_4$ matrix.

The shift of the peak position in the X-ray diffraction can be attributed to the change of the lattice constants of the unit cell of the studied system. The doping or substitution of ions in the matrix with an ion of different size can cause tensile compressive strain in the unit cell. This may result in expansion or shrinking of the unit cell depending on the ionic radius of the dopant. In this case, the positions of diffraction peaks slightly shifted to lower diffraction angles due to the reduction of the interplanar spacing because of the substitution of the larger radius Gd^{3+} ions (1.053 Å) by the smaller Er^{3+} (1.004 Å) and Yb^{3+} (0.985 Å) ions (for coordination VIII) [37]. The structural parameters of the sample were evaluated from the XRD data and the obtained average crystallite size was about 15 nm. A lower-magnification TEM image measured on a grid coated with nanoparticles dispersed in ethanol is shown in Fig. 2b. The TEM image shows that the synthesized $GdVO_4$:Er^{3+}/Yb^{3+} nanoparticles are mostly elliptic with size of about 30 nm.

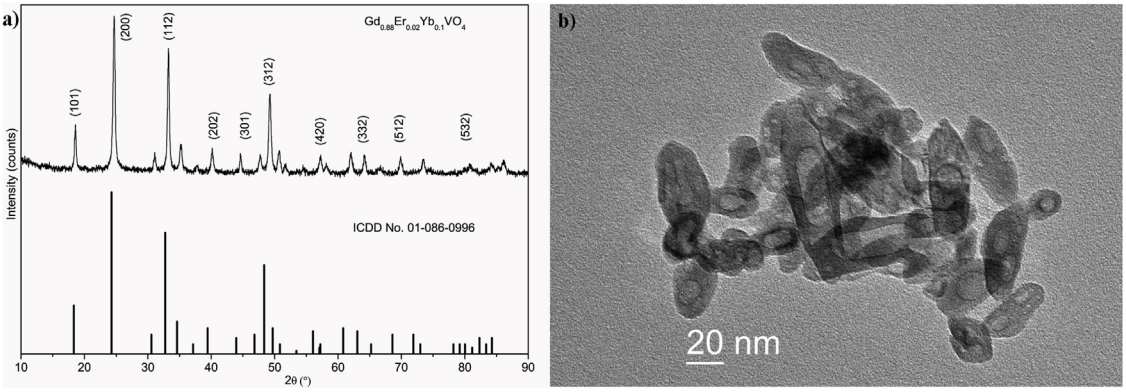

Fig. 2. (a) XRD pattern and (b) TEM image for $Gd_{0.88}Er_{0.02}Yb_{0.1}VO_4$ powder.

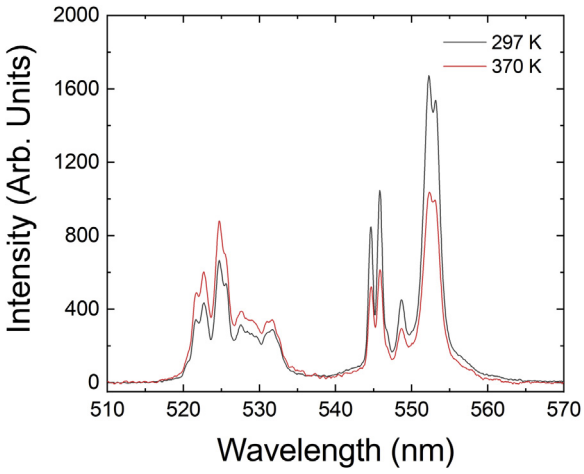

Fig. 3. Emission spectra of GdVO4: Er^{3+}/Yb^{3+} at two different temperatures after excitation at 457 nm.

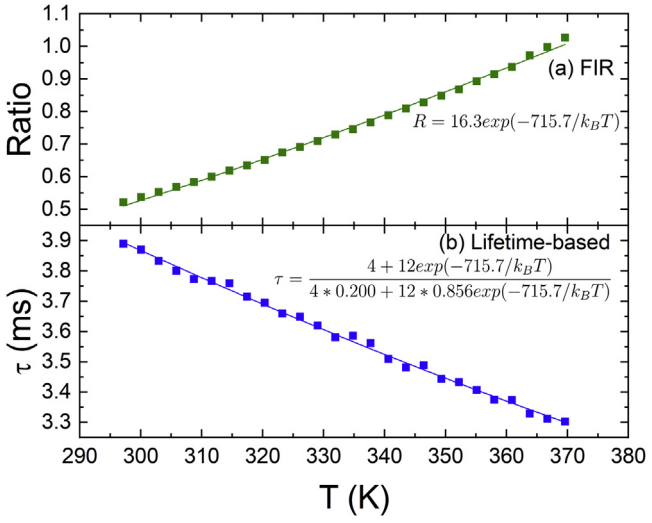

Fig. 4. Temperature calibrations of the down-conversion emissions of GdVO4: Er^{3+}/Yb^{3+} through (a) FIR technique and (b) fluorescence lifetime-based calibration.

4.2. FIR temperature calibration

When the sample was excited with a 457 nm continuous laser, in resonance with the $^4I_{15/2} \rightarrow {}^4F_{5/2}$ and $^4I_{15/2} \rightarrow {}^4F_{3/2}$ transition, a bright green emission can be observed by the naked eye. The green emission is associated to the two coupled energy levels centered at around 525 nm and 550 nm corresponding to the transitions from the $^2H_{11/2}$ and $^4S_{3/2}$ levels to the $^4I_{15/2}$ ground state, respectively. Fig. 3 presents the down-conversion spectra for two different temperatures. As can be seen, as the temperature increases, the population in the lower level ($^4S_{3/2}$) decreases while the population in the upper level ($^2H_{11/2}$) increases. This intensity evolution confirms that the energy levels $^4S_{3/2}$ and $^2H_{11/2}$ are thermally coupled.

The change in the intensity ratio of the 525 nm band over the 550 nm band is plotted against the absolute temperature and it is shown in Fig. 4a. It can be seen that the FIR varied from 0.52 to 1.03 as the temperature increased from 297 to 370 K. The data are fitted according to Eq. (3) with an exponential function and an energy gap ΔE=715.7 cm^{-1} and a pre-exponential of about 16.3 were obtained. This energy gap is in accordance with the one obtained from the FIR calibration of a similar sample but using an excitation of about 980 nm and involving upconversion mechanisms [28].

4.3. Lifetime-based temperature calibration

The decay curves of the nanoparticles under the excitation of a pulsed 457 nm laser for two different temperatures where shown in Fig. 5. To obtain the effective lifetime for each temperature, the decay curves are fitted to the exponential decay equation: $I(t)/I_0 = \exp(-t/\tau)$, wherein $I(t)$ and I_0 are the intensity at time t and $t=0$, respectively, and τ is the effective lifetime [38]. As can be observed, the effective fluorescence lifetime decreases with increasing temperature. The effective lifetimes for different temperatures are shown in Fig. 4b. and fitted according to Eq. (4), wherein the pre-

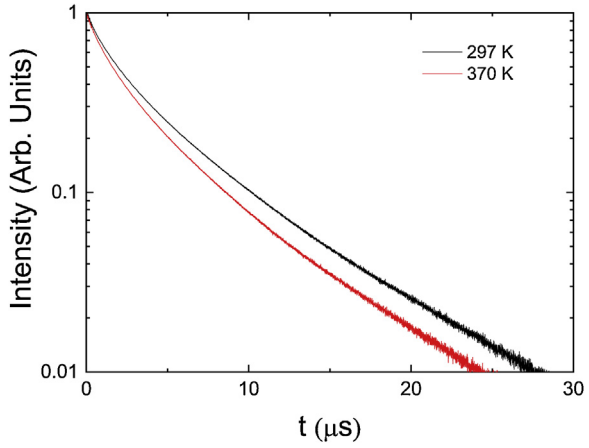

Fig. 5. Decay curves of the thermally-coupled energy levels of Er^{3+} for two different temperatures.

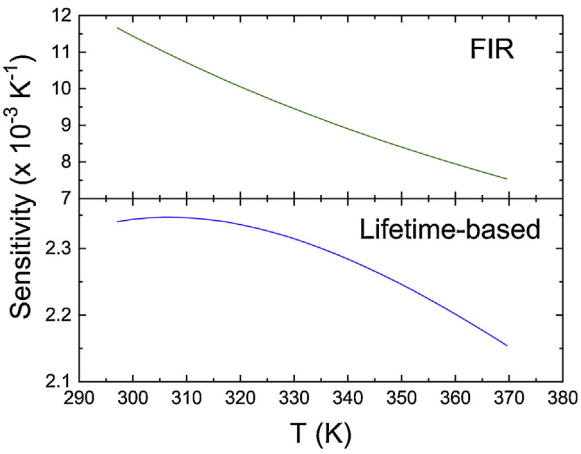

Fig. 6. Relative sensitivity of the (a) FIR-based and (b) lifetime-based sensor.

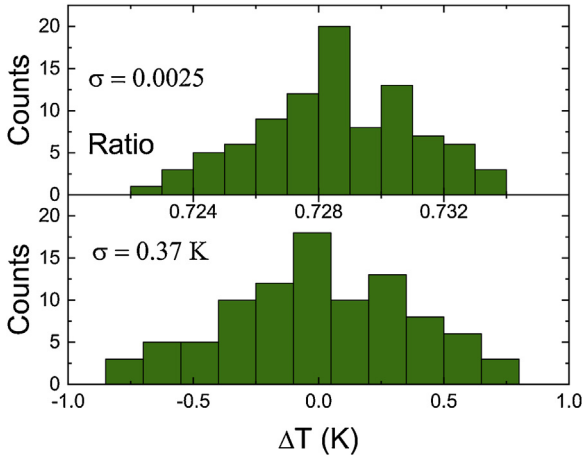

Fig. 7. Distributions of the intensity ratio and temperature of GdVO4: Er^{3+}/Yb^{3+} sample using the FIR technique.

viously obtained ΔE is used, leaving A_1 and A_2 as free parameters. Level 1 corresponds to $^4S_{3/2}$ and level 2 corresponds to $^2H_{11/2}$. The probabilities of spontaneous emission A_1 and A_2 obtained from the fit are 200 s^{-1} and 856 s^{-1} respectively. Therefore, the intrinsic lifetime of the two levels are as follows: $\tau_1 = 5.0$ ms and $\tau_2 = 1.2$ ms. As previously explained, a decreasing lifetime was observed with the temperature. The upper level ($^2H_{11/2}$) has a shorter lifetime and due to the increase of the temperature this level is populated and the effective lifetime decreases (Eq. (4)).

4.4. Relative sensitivity

In order to determine the sensing method to be used for the electrical component, the relative sensitivity of each method was calculated according to Eqs. (6) and (7) and are represented in Fig. 6. The maximum sensitivity for the FIR technique was achieved at the lowest temperature of 297 K with a value of 1.17% K^{-1}. This value is comparable to previously obtained values from the literature such as for $CaWO_4$: Er^{3+}/Yb^{3+} phosphor (1.00% K^{-1} at 300 K) [39], Er^{3+} doped oxysulfide powder (1.09% K^{-1} at 300 K) [40], and $NaBiF_4$: Er^{3+}/Yb^{3+} nanoparticle (1.24% K^{-1} at 303 K) [41]. On the other hand, the maximum sensitivity for the lifetime-based calibration does not correspond to the lowest temperature, rather at 306 K with a value of 0.24% K^{-1}. As can be observed, for the same range of temperatures, the sensitivities of the FIR-based sensor are higher than those of the lifetime-based. For this reason, the FIR technique was chosen for the study of the temperature of the electrical component.

To determine the temperature uncertainty of FIR temperature measurements, 100 spectra of the nanoparticles were obtained under the same conditions. Afterwards, the intensity ratio and temperature were calculated according to the FIR method and the distributions were represented in Fig. 7. The temperature uncertainty for this method, taken as the standard deviation of the temperature distribution, is found to be 0.37 K. This is better than the one obtained with erbium-doped lanthanum oxysulfide powders [40].

4.5. Temperature of the electrical component

A conventional non-contact way of measuring the temperature of an object is with the use of an infrared camera. An infrared image of the electrical component connected to a power supply is shown in Fig. 8. The figure shows a temperature value of 59 °C obtained approximately in the center of the electrical component when it is operating.

The response time of infrared cameras depend on the thermal time constant τ_{TH} of the bolometer, which for the infrared camera

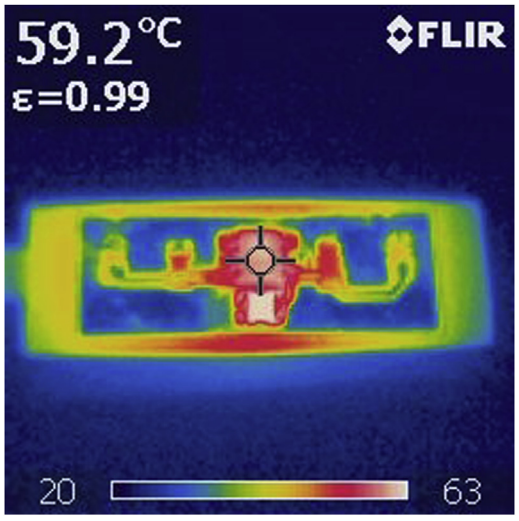

Fig. 8. Infrared image of the electrical component connected to a power supply.

employed is around 7 to 12 ms. Since the rate of heating up or cooling down is given as $1 - e^{-t/\tau_{TH}}$, approximately a minimum of three τ_{TH} (21 ms) are needed to represent 95% of the input signal. On the other hand, the thermalization of the coupled energy levels for the FIR technique can be evaluated much faster, from a couple of femtoseconds to picoseconds after the excitation [42]. Furthermore, another disadvantage of infrared cameras is that it has poor spatial resolution not better than 10 μm while spatial resolutions below 500 nm has been obtained for a PbF_2: Er^{3+}/Yb^{3+} nanoparticles using the FIR technique [43].

Therefore, using the FIR method, the temperature of the nanoparticles distributed on the surface of the electrical component was measured for 100 min. During this time, the component was connected and disconnected to a power supply. The temporal evolution of the temperature is shown in Fig. 9. It can be seen from the graph that when the component was connected to a power supply, the component heated from RT to 58 °C (331 K) in 20 min. When it was disconnected, the component cooled off to RT in 15 min. Moreover, the temperature measured by the FIR when the electrical component is operating (about 58 °C) is in accordance with the one measured by the infrared camera (about 59 °C).

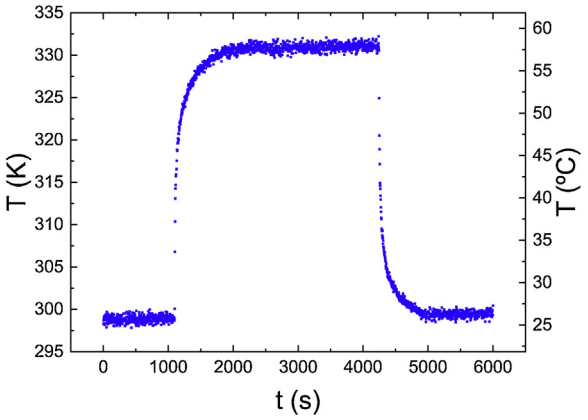

Fig. 9. Temporal evolution of the temperature of an electrical component when it is connected and disconnected to a power supply.

5. Conclusions

The application of $GdVO_4$: Er^{3+}/Yb^{3+} as a temperature sensor was studied using the FIR technique and the fluorescence lifetime-based calibration. Using the FIR technique, intensity ratio of the 525 nm and 550 nm emission bands were calibrated with the temperature. An energy gap of 715.7 cm^{-1} was obtained for the $^4S_{3/2}$ and $^2H_{11/2}$ energy levels. Using this value, the effective lifetime of these levels were also calibrated with temperature and probabilities of spontaneous emission from the $^4S_{3/2}$ and $^2H_{11/2}$ levels were obtained as 200 s^{-1} and 856 s^{-1} respectively. The relative sensitivity for both methods was calculated and the FIR method provided higher sensitivity than the lifetime-based method, with a maximum value of 1.17% K^{-1} at 297 K. For this reason, FIR technique was used to observe the temporal evolution of the temperature of an electric component when it is operating and it is partially covered with $GdVO_4$: Er^{3+}/Yb^{3+} nanoparticles. The value of temperature of this electrical component obtained using FIR technique is in agreement with the value obtained using an infrared camera. However, it is expected that with the $GdVO_4$: Er^{3+}/Yb^{3+} nanoparticles used as optical sensors, it is possible to obtain better spatial and temporal resolutions than the infrared camera.

Funding

This research was partially supported by the Spanish MINECO [MAT2015-71070-REDC, and MAT2016-75586-C4-4-P, FIS2016-77319-C2-1-R], and by the EU-FEDER funds. L. Martin acknowledges the support from the Spanish Juan de la Cierva program [IJCI-2016-30498]. The D. Jovanović also acknowledges the financial support of the Ministry of Education, Science and Technological Development of the Republic of Serbia [Project no: 172056].

References

[1] M. Haouari, A. Maaoui, N. Saad, A. Bulou, Optical temperature sensing using green emissions of Er^{3+} doped fluoro-tellurite glass, Sens. Actuators A Phys. (2017), http://dx.doi.org/10.1016/j.sna.2017.04.012.
[2] V. Klinkov, V. Aseev, A. Semencha, E. Tsimerman, Temperature sensor based on upconversion luminescence of Er^{3+}-doped fluoroaluminate glasses, Sens. Actuators A Phys. (2018), http://dx.doi.org/10.1016/j.sna.2018.04.048.
[3] W. Xu, H. Zhao, Z. Zhang, W. Cao, Highly sensitive optical thermometry through thermally enhanced near infrared emissions from Nd^{3+}/Yb^{3+} codoped oxyfluoride glass ceramic, Sens. Actuators B Chem. (2013), http://dx.doi.org/10.1016/j.snb.2012.12.050.
[4] J. Liao, Q. Wang, L. Lan, J. Guo, L. Nie, S. Liu, H.R. Wen, Microwave hydrothermal synthesis and temperature sensing behavior of $Lu_2Ti_2O_7$:Yb^{3+}/Er^{3+} nanophosphors, Curr. Appl. Phys. (2017), http://dx.doi.org/10.1016/j.cap.2017.01.005.
[5] L. Tong, X. Li, R. Hua, L. Cheng, J. Sun, J. Zhang, S. Xu, H. Zheng, Y. Zhang, B. Chen, Optical temperature sensing properties of Yb^{3+} /Tm^{3+} co-doped $NaLuF_4$ crystals, Curr. Appl. Phys. (2017), http://dx.doi.org/10.1016/j.cap.2017.03.021.
[6] W.A. Pisarski, J. Pisarska, R. Lisiecki, W. Ryba-Romanowski, $Er3^+/Yb^{3+}$ co-doped lead germanate glasses for up-conversion luminescence temperature sensors, Sens. Actuators A Phys. (2016), http://dx.doi.org/10.1016/j.sna.2016.11.010.
[7] X. Wang, X. Li, S. Xu, L. Cheng, J. Sun, J. Zhang, B. Chen, Can temperature be accurately sensed by red-green emission ratio in $YNbO_4$: Ho^{3+}/Yb^{3+} phosphor under 980 nm excitation? J. Alloys Compd. (2018), http://dx.doi.org/10.1016/j.jallcom.2018.04.299.
[8] N. Vijaya, P. Babu, V. Venkatramu, C.K. Jayasankar, S.F. León-Luis, U.R. Rodríguez-Mendoza, I.R. Martín, V. Lavín, Optical characterization of Er^{3+}-doped zinc fluorophosphate glasses for optical temperature sensors, Sens. Actuators B Chem. (2013), http://dx.doi.org/10.1016/j.snb.2013.05.081.
[9] F. Huang, Y. Gao, J. Zhou, J. Xu, Y. Wang, Yb^{3+}/Er^{3+} co-doped CaMoO4: A promising green upconversion phosphor for optical temperature sensing, J. Alloys Compd. (2015), http://dx.doi.org/10.1016/j.jallcom.2015.02.228.
[10] C. Li, B. Dong, S. Li, C. Song, Er^{3+}-Yb^{3+} co-doped silicate glass for optical temperature sensor, Chem. Phys. Lett. (2007), http://dx.doi.org/10.1016/j.cplett.2007.06.081.
[11] A.K. Soni, V.K. Rai, M.K. Mahata, Yb^{3+} sensitized $Na_2Y_2B_2O_7$:Er^{3+} phosphors in enhanced frequency upconversion, temperature sensing and field emission display, Mater. Res. Bull. (2017), http://dx.doi.org/10.1016/j.materresbull.2017.01.009.
[12] H. Song, C. Wang, Q. Han, X. Tang, W. Yan, Y. Chen, J. Jiang, T. Liu, Highly sensitive Tm^{3+}/Yb^{3+} codoped $SrWO_4$ for optical thermometry, Sens. Actuators A Phys. (2018), http://dx.doi.org/10.1016/j.sna.2018.01.037.
[13] T. Sun, Z.Y. Zhang, K.T.V. Grattan, A.W. Palmer, Ytterbium-based fluorescence decay time fiber optic temperature sensor systems, Rev. Sci. Instrum. (1998), http://dx.doi.org/10.1063/1.1149267.
[14] Z.Y. Zhang, K.T.V. Grattan, B.T. Meggitt, Thulium-doped fiber optic decay-time temperature sensors: characterization of high temperature performance, Rev. Sci. Instrum. (2000), http://dx.doi.org/10.1063/1.1150506.
[15] Y. Shen, W. Zhao, J. He, T. Sun, K.T.V. Grattan, Fluorescence decay characteristic of Tm-doped YAG crystal fiber for sensor applications, investigated from room temperature to 1400°C, IEEE Sens. J. (2003), http://dx.doi.org/10.1109/JSEN.2003.815772.
[16] D. Chen, S. Liu, X. Li, S. Yuan, P. Huang, Upconverting luminescence based dual-modal temperature sensing for $Yb^{3+}/Er^{3+}/Tm^{3+}$: YF_3 nanocrystals embedded glass ceramic, J. Eur. Ceram. Soc. (2017), http://dx.doi.org/10.1016/j.jeurceramsoc.2017.06.012.
[17] H. Lu, H. Hao, Y. Gao, G. Shi, Q. Fan, Y. Song, Y. Wang, X. Zhang, Dual functions of Er^{3+}/Yb^{3+} codoped $Gd_2(MoO_4)_3$ phosphor: temperature sensor and optical heater, J. Lumin. (2017), http://dx.doi.org/10.1016/j.jlumin.2016.12.026.
[18] D.K. Singh, J. Manam, Efficient dual emission mode of green emitting perovskite $BaTiO_3$: Er^{3+} phosphors for display and temperature sensing applications, Ceram. Int. (2018), http://dx.doi.org/10.1016/j.ceramint.2018.03.151.
[19] D. Jia, Z. Yuan, H. San, L. Gao, The study of fluorescence thermal measurement based on DSP, Procedia Eng. 29 (2012) 2864–2868, http://dx.doi.org/10.1016/j.proeng.2012.01.405.
[20] W.P. Chen, F.F. Hu, R.F. Wei, Q.G. Zeng, L.P. Chen, H. Guo, Optical thermometry based on up-conversion luminescence of Tm^{3+} doped transparent Sr_2YF_7 glass ceramics, J. Lumin. (2017), http://dx.doi.org/10.1016/j.jlumin.2017.07.002.
[21] M.K. Mahata, K. Kumar, V.K. Rai, Er^{3+}–Yb^{3+} doped vanadate nanocrystals: A highly sensitive thermographic phosphor and its optical nanoheater behavior, Sens. Actuators B Chem. (2015), http://dx.doi.org/10.1016/j.snb.2014.12.039.
[22] B. Lai, L. Feng, J. Wang, Q. Su, Optical transition and upconversion luminescence in Er^{3+} doped and Er^{3+}-Yb^{3+} co-doped fluorophosphate glasses, Opt. Mater. (Amst). (2010), http://dx.doi.org/10.1016/j.optmat.2010.03.023.
[23] D. Wang, N. Kodama, Visible quantum cutting through downconversion in $GdPO_4$:Tb^{3+} and $Sr_3Gd(PO_4)_3$:Tb^{3+}, J. Solid State Chem. (2009), http://dx.doi.org/10.1016/j.jssc.2009.05.026.
[24] B. Dong, B.S. Cao, Z.Q. Feng, X.J. Wang, Y.Y. He, Optical temperature sensing through extraordinary enhancement of green up-conversion emissions for Er-Yb-Mo:Al_2O_3, Sens. Actuators B Chem. (2012), http://dx.doi.org/10.1016/j.snb.2012.01.068.
[25] Y. Liang, H.M. Noh, J. Xue, H. Choi, S.H. Park, B.C. Choi, J.H. Kim, J.H. Jeong, High quality colloidal $GdVO_4$:Yb,Er upconversion nanoparticles synthesized via a protected calcination process for versatile applications, Mater. Des. (2017), http://dx.doi.org/10.1016/j.matdes.2017.05.058.
[26] J.H. Oh, B.K. Moon, B.C. Choi, J.H. Jeong, J.H. Kim, H.S. Lee, The green upconversion emission mechanism investigation of $GdVO_4$:Yb^{3+}, Er^{3+} via tuning of the sensitizer concentration, Solid State Sci. (2015), http://dx.doi.org/10.1016/j.solidstatesciences.2015.02.010.
[27] D.J. Jovanović, T.V. Gavrilović, S.D. Dolić, M. Marinović-Cincović, K. Smits, M.D. Dramićanin, Up-conversion luminescence of $GdVO_4$:Nd^{3+}/Er^{3+} and $GdVO_4$:Nd^{3+}/Ho^{3+} phosphors under 808 nm excitation, Opt. Mater. (Amst). (2018), http://dx.doi.org/10.1016/j.optmat.2018.05.033.
[28] T.V. Gavrilović, D.J. Jovanović, V. Lojpur, M.D. Dramićanin, Multifunctional Eu^{3+}- and Er^{3+}/Yb^{3+}-doped $GdVO_4$ nanoparticles synthesized by reverse micelle method, Sci. Rep. 4 (2014) 1–9, http://dx.doi.org/10.1038/srep04209.
[29] O.A. Savchuk, J.J. Carvajal, C. Cascales, M. Aguiló, F. Díaz, Benefits of silica core-shell structures on the temperature sensing properties of Er,Yb:$GdVO_4$

up-conversion nanoparticles, ACS Appl. Mater. Interfaces (2016), http://dx.doi.org/10.1021/acsami.6b01371.
[30] A.K. Singh, Ho^{3+}:TeO_2 glass, a probe for temperature measurements, Sens. Actuators A Phys. (2007), http://dx.doi.org/10.1016/j.sna.2006.10.045.
[31] H. Zheng, B. Chen, H. Yu, X. Li, J. Zhang, J. Sun, L. Tong, Z. Wu, H. Zhong, R. Hua, H. Xia, Rod-shaped $NaY(MoO_4)_2$:Sm^{3+}/Yb^{3+} nanoheaters for photothermal conversion: Influence of doping concentration and excitation power density, Sens. Actuators B Chem. 234 (2016) 286–293, http://dx.doi.org/10.1016/j.snb.2016.04.162.
[32] Y. Zhang, B. Chen, S. Xu, X. Li, J. Zhang, J. Sun, X. Zhang, H. Xia, R. Hua, A universal approach for calculating the Judd–Ofelt parameters of RE^{3+} in powdered phosphors and its application for the β-$NaYF_4$:Er^{3+}/Yb^{3+} phosphor derived from auto-combustion-assisted fluoridation, Phys. Chem. Chem. Phys. 20 (2018) 15876–15883, http://dx.doi.org/10.1039/C8CP02317D.
[33] V.K. Rai, Temperature sensors and optical sensors, Appl. Phys. B Lasers Opt. 88 (2007) 297–303, http://dx.doi.org/10.1007/s00340-007-2717-4.
[34] S.F. Collins, G.W. Baxter, S.A. Wade, T. Sun, K.T.V. Grattan, Z.Y. Zhang, A.W. Palmer, Comparison of fluorescence-based temperature sensor schemes: theoretical analysis and experimental validation, J. Appl. Phys. 84 (1998) 4649–4654, http://dx.doi.org/10.1063/1.368705.
[35] C.D.S. Brites, A. Millán, L.D. Carlos, Lanthanides in luminescent thermometry, in: Handb. Phys. Chem. Rare Earths, 2016, pp. 339–427, http://dx.doi.org/10.1016/bs.hpcre.2016.03.005.
[36] T.V. Gavrilović, D.J. Jovanović, K. Smits, M.D. Dramićanin, Multicolor upconversion luminescence of $GdVO_4$:Ln^{3+}/Yb^{3+}(Ln^{3+}= Ho^{3+}, Er^{3+}, Tm^{3+}, Ho^{3+}/Er^{3+}/Tm^{3+}) nanorods, Dyes Pigm. 126 (2016) 1–7, http://dx.doi.org/10.1016/j.dyepig.2015.11.005.
[37] R.D. Shannon, Revised effective ionic radii and systematic studies of interatomic distances in halides and chalcogenides, Acta Crystallogr. Sect. A (1976), http://dx.doi.org/10.1107/S0567739476001551.
[38] D.K. Singh, J. Manam, Efficient dual emission mode of green emitting perovskite $BaTiO_3$: Er^{3+} phosphors for display and temperature sensing applications, Ceram. Int. 44 (2018) 10912–10920, http://dx.doi.org/10.1016/j.ceramint.2018.03.151.
[39] X. Cheng, K. Yang, J. Wang, L. Yang, X. Cheng, Up-conversion luminescence and optical temperature sensing behaviour of Yb^{3+}/Er^{3+} codoped $CaWO_4$ material, Opt. Mater. (Amst). 58 (2016) 449–453, http://dx.doi.org/10.1016/j.optmat.2016.06.029.
[40] R. Balda, N. Hakmeh, M. Barredo-Zuriarrain, O. Merdrignac-Conanec, S. García-Revilla, M.A. Arriandiaga, J. Fernández, Influence of upconversion processes in the optically-induced inhomogeneous thermal behavior of erbium-doped lanthanum oxysulfide powders, Materials (Basel) (2016), http://dx.doi.org/10.3390/ma9050353.
[41] P. Du, L. Luo, X. Huang, J.S. Yu, Ultrafast synthesis of bifunctional Er^{3+}/Yb^{3+}-codoped $NaBiF_4$ upconverting nanoparticles for nanothermometer and optical heater, J. Colloid Interface Sci. 514 (2018) 172–181, http://dx.doi.org/10.1016/j.jcis.2017.12.027.
[42] N. Terzi, M. Dominoni, Ultrafast electron-lattice relaxation of optically excited centers in crystals, in: B. Di Bartolo, G. Gambarota (Eds.), Ultrafast Dyn. Quantum Syst. Phys. Process. Spectrosc. Tech., Springer US, Boston, MA, 2002, pp. 569–582, http://dx.doi.org/10.1007/0-306-47080-2_20.
[43] C.D.S. Brites, P.P. Lima, N.J.O. Silva, A. Millán, V.S. Amaral, F. Palacio, L.D. Carlos, Thermometry at the nanoscale, Nanoscale (2012), http://dx.doi.org/10.1039/c2nr30663h.

Biographies

Franzette Paz-Buclatin graduated in Physics in 2018 from the University of La Laguna. She is currently working as part of the Laser Spectroscopy and High Pressure group. Her research interests cover optical temperature sensors and optical microresonators.

Fernando Rivera-López is Professor at the Department of Industrial Engineering at the University of La Laguna. He received a PhD in 2011 from University of La Laguna. He is a member of the Laser Spectroscopy and High Pressure group. He is currently involved in the optical characterization of crystals, glasses and glass-ceramics doped with rare-earth ions.

Oswaldo González is a senior lecturer in the department of Industrial Engineering at University of La Laguna (Spain). He obtained his M.S. degree in Electronics Engineering from this same university in 2000, achieving his Ph.D. on optical wireless communications (OWC) in 2005. His main research interests are in the field of optical wireless channel characterization, orthogonal frequency division multiplexing (OFDM) for multi-user OWC, optical code-division multiple access (OCDMA) and visible light communications (VLC), issues about which he has published several papers in international journals (IEEE, IEE/IET, OSA) and a book chapter about multiple-input multiple-output (MIMO) optical wireless communications.

Inocencio R. Martín is Full Professor at the Department of Physics at the University of La Laguna, Spain. He received a Ph.D. in 1996 from the University of La Laguna. He is a member of the Laser Spectroscopy and High Pressure group and the MALTA Project and his research interests cover the optical characterization of glasses, crystals and nanocrystalline glass-ceramics doped with optically active ions. He has over 200 publications in peer reviewed journals. Currently, he is involved in optical characterization of microspheres doped with rare-earth ions and in new nanomaterials in order to be used in different applications.

Leopoldo L. Martin received his PhD in 2013 and is now a "Juan de la Cierva" Fellow at the University of La Laguna. His current research field is applied photonics and the use of fluorescent optical microresonators as sensors and as a test bench for quantum optics.

Dragana J. Jovanović received her PhD in 2010 at the Faculty of Physical Chemistry, University of Belgrade, Serbia. She has been employed in the Vinča Institute of Nuclear Sciences, University of Belgrade, Serbia, from 2006. Now, she has position of Senior Research Fellow at Vinča Institute of Nuclear Sciences, University of Belgrade. Her research is focused on the synthesis and characterization of optical (nano) materials for use in chemical and thermal sensing including spectroscopic methods. She has (co-)authored more than 50 papers (h-index: 19), and number of citation is about 1100 (Google Scholar, June 2019).